Numerical simulations of a non-conservative hyperbolic system with geometric constraints describing swarming behavior

Sebastien Motsch[*]   Laurent Navoret[†‡]

June 3, 2011

Abstract

The Vicsek model is a very popular individual based model which describes collective behavior among animal societies. A large-scale limit of the Vicsek model has been derived in [16] leading to a macroscopic version of the model. In this work, we want to numerically validate this Macroscopic Vicsek (MV) model. However, there is no standard theory to study analytically or numerically the MV model since it is a non-conservative hyperbolic system with a geometric constraint. Different formulations of the MV model are presented and lead to several non-equivalent numerical schemes. In particular, we derive a numerical scheme, denoted by the *splitting method*, based on a relaxation of the geometric constraint. To test the veracity of these schemes, we compare the simulations of the macroscopic and microscopic models with each other. The numerical simulations reveal that the microscopic and macroscopic models are in good agreement, provided that we use the *splitting method* to simulate the MV model. This result confirms the relevance of the macroscopic model but it also calls for a better theoretical understanding of this type of equations.

---

[*]Center of Scientific Computation and Mathematical Modeling (CSCAMM), University of Maryland, College Park, MD 20742, USA, `smotsch@cscamm.umd.edu`

[†]Université de Toulouse, UPS, INSA, UT1, UTM, Institut de Mathématiques de Toulouse, F-31062 Toulouse, France, `laurent.navoret@math.univ-toulouse.fr`

[‡]CNRS, Institut de Mathématiques de Toulouse UMR 5219, F-31062 Toulouse, France

1 Introduction

The modeling of swarming behavior has received considerable attention in recent years. There are currently two types of approach which are used to model collective behavior. First, there is a wide range of "microscopic" models, also called individual based models in biology, which describe the motion of each individual separately. For example, this type of model is used in the modeling of a flock of birds [3] or a school of fish [2, 11, 26, 32]. Since collective behavior in a natural environment can concern up to several million individuals, another type of model called "macroscopic" model is also in use [10, 30]. In this kind of model, the swarm is described by macroscopic variables (e.g. mean density, mean velocity). On the one hand, macroscopic models constitute powerful analytical tools to study the dynamics at large scales [16–18, 33]. On the other hand, the related numerical schemes are computationally much more efficient compared with particle simulations of a large number of interacting agents. The price to pay is that finding accurate numerical schemes for a macroscopic model requires much more work compared to a microscopic model.

Among all the individual based models used in biology, the so-called Vicsek model [35] has received particular attention [4]. In this model, individuals are moving at a constant speed and tend to align with their neighbors. From this simple local rule emerges a collective coherent motion. Due to its simplicity, this model has been used to describe several phenomena, such as the motion of locusts [6] or the motion of birds [3]. From a theoretical point of view, many questions remain open about it. A first field of research concerns phase transitions within the model depending on the level of noise [1, 8, 14, 15, 22, 31, 35]. Another question arises from the long time dynamics of the model [12, 13, 23]: does the system convergence to a stationary state? To study the dynamics of the Vicsek model at large scales, it is useful to derive a macroscopic limit of this model. For this reason, a macroscopic limit, called Macroscopic Vicsek (MV) model, has been derived in [16]. The macroscopic model is obtained from a rigorous perturbation theory of the original Vicsek model. However, to make this macroscopic model effective, we need to know how to simulate this model. Only then it will be possible to explore the large scale

behavior of the Vicsek model from another point of view.

The MV model presents several characteristics which make its numerical simulation challenging. First, it is a non-conservative hyperbolic system, and secondly, it involves a geometric constraint. These are the consequences at the macroscopic level of two properties of the microscopic model: the total momentum is not conserved by the particle dynamics and the speed of the particles is constant. We would like to emphasize that these two properties are not specific to the Vicsek model. Indeed, many models of self-propelled particles do not preserve the total momentum. The assumption that particles are moving at a constant speed is also a usual assumption in the modeling of collective displacements [11, 21, 35]. Up to our knowledge, the theory of non-conservative hyperbolic systems with geometric constraint is almost empty. Non-conservative systems have been studied in various literature [5, 7, 9, 25, 27] but none of them involve geometric constraints. Therefore, since a theoretical framework for the MV model is not available, how can we simulate such a model? More importantly, how can we validate the numerical results?

In this work, we propose several approaches to solve numerically the MV model. First, we notice in 1D that the MV model can be transformed into a conservative system. This formulation enables the use of the standard hyperbolic theory to simulate the system. This yields our first numerical scheme called the *conservative method*. Moreover, we use this conservative formulation to find analytically shock wave solutions. But manipulation of conservation laws can be delicate: the equivalence between the conservative formulation and the MV model is only valid for smooth functions. There is no guarantee that the shock waves found using the conservative formulation are also solutions to the original MV model. For this reason, it is essential to develop other approaches. We propose a second formulation of the MV model where the geometric constraint is replaced by a relaxation operator. In this formulation, the MV model is seen as the relaxation limit of an unconstrained conservative system. This formulation leads naturally to a numerical scheme based on a splitting between the conservative part of the equation and the relaxation part. This scheme is referred to as the *splitting method*. For comparison purposes, two simple discretizations of the MV model are also introduced: the *upwind scheme* and the *semi-conservative* scheme.

To test our four numerical schemes, we simulate the MV model with several initial conditions. To begin, we use an initial condition where the theoretical solution is given by a rarefaction wave. All four schemes effectively capture the rarefaction wave. In contrast, when we use an initial condition where the theoretical solution should be a shock wave, the four schemes are in complete disagreement. To determine the "correct solution", we run particle simulations of the microscopic model. For instance, when the number of particles per domain of interaction is high, micro-

scopic and macroscopic models are close to each other. The numerical simulations reveal, unexpectedly, that only the splitting method is in good agreement with the microscopic simulations. This is even clearer when we start our initial condition with a contact discontinuity. The solution given by the conservative method is simply a convection of the initial condition whereas the splitting method and the particle simulations agree on a different and more complex solution.

These numerical results answer two questions at once. First, the MV model describes accurately the microscopic model in a dense regime of particles. Secondly, the correct formulation of the MV model is given by the limit of a conservative model with a stiff relaxation term. But these theoretical and numerical studies of the MV model also highlight the specificity of non-conservative hyperbolic models with geometric constraints. More theoretical work is necessary to understand why the splitting method matches the microscopic model and why other methods do not. An extension of the theory developed in [9] to non-conservative relaxed models would be particularly desirable.

The outline of the paper is as follows: we introduce the microscopic and macroscopic Vicsek models in section 2. Next, we analyze the MV model and give two different formulations of the model in section 3. We develop different numerical schemes based on these formulations in section 4 and solve numerically different Riemann problems. In section 5, we compare the simulations of the microscopic model with those of the macroscopic model. Finally, a conclusion is drawn in section 6.

2 Presentation of the Vicsek and Macroscopic Vicsek models

In this section, we briefly present the Vicsek model at the microscopic and macroscopic scale. We refer the reader interested in the derivation of the macroscopic model to [16].

At the particle level, the Vicsek model describes the motion of particles which tend to align with their neighbors. Each particle is represented by a position vector x_k and a velocity ω_k with a constant speed ($|\omega_k| = 1$). To simplify, we suppose that the particles move in a plane, thus $x_k \in \mathbb{R}^2$ and $\omega_k \in \mathbb{S}^1$. The Vicsek model at the microscopic level is given by the following equations (in dimensionless variables):

$$\frac{dx_k}{dt} = \omega_k, \tag{2.1}$$

$$d\omega_k = (\mathrm{Id} - \omega_k \otimes \omega_k)(\overline{\omega}_k \, dt + \sqrt{2d} \, dB_t), \tag{2.2}$$

where Id is the identity matrix and the symbol $\otimes$ denotes the tensor product of vectors. Here, d is the intensity of noise, B_t is the Brownian motion and $\overline{\omega}_k$ is the

direction of the mean velocity around the particle k,

$$\overline{\omega}_k = \frac{J_k}{|J_k|} \,, \qquad J_k = \sum_{j,\,|x_j - x_k| \leq R} \omega_j, \tag{2.3}$$

where R defines the radius of the interaction region. Taken together, equations (2.2) and (2.3) express the tendency of particles to move in the same direction as their neighbors. The operator $(\text{Id} - \omega_k \otimes \omega_k)$ is the orthogonal projector onto the plane perpendicular to ω_k. It ensures that the speed of particles remains constant. This model is already a modification of the original Vicsek model [35] which is a time-discrete algorithm.

The Macroscopic Vicsek model (MV) describes the evolution of two macroscopic quantities: the density of particles ρ and the direction of the flow Ω. The evolution of ρ and Ω is governed by the system:

$$\partial_t \rho + \nabla_x \cdot (c_1 \rho \Omega) = 0, \tag{2.4}$$

$$\rho \left(\partial_t \Omega + c_2 (\Omega \cdot \nabla_x) \Omega \right) + \lambda \, (\text{Id} - \Omega \otimes \Omega) \nabla_x \rho = 0, \tag{2.5}$$

$$|\Omega| = 1, \tag{2.6}$$

where c_1, c_2 and λ are constants depending on the noise parameter d. The expressions of c_1, c_2 and λ are given in appendix A. In contrast to the standard Euler system, the two convection coefficients c_1 and c_2 are different. The other specificity of this model is the constraint $|\Omega| = 1$. The operator $(\text{Id} - \Omega \otimes \Omega)$ ensures that this constraint is propagated provided that it is true initially. We note that vortex configurations are special stationary solutions of this model in two dimensions (see appendix B). Up to our knowledge, this is the first swarming model that has such analytical solutions.

3   The Macroscopic Vicsek model

To devise numerical schemes for the MV model, we present several formulations of this model that will suggest different numerical methods. As we will see, the MV model is strictly hyperbolic but it is also a non-conservative system, and therefore classical finite volume schemes are not necessarily well-adapted. For this reason, we introduce two "conservative" formulations of the MV model that will lead to more robust numerical schemes.

3.1   Theoretical analysis of the macroscopic model

Event though the MV model is not a classical system of conservation laws, some general properties can be obtained analytically. In particular, we deduce explicit

one dimensional solutions of the system (the so-called rarefaction waves). These solutions will be used later to test the accuracy of the numerical schemes.

To study the system (2.4)-(2.6), it is more convenient to use the rescaling $x' = x/c_1$. Thus equations (2.4)-(2.6) read:

$$\partial_t \rho + \nabla_{x'} \cdot (\rho \Omega) = 0, \tag{3.1}$$

$$\rho \left(\partial_t \Omega + c'(\Omega \cdot \nabla_{x'})\Omega \right) + \lambda' \left(\text{Id} - \Omega \otimes \Omega \right) \nabla_{x'} \rho = 0, \tag{3.2}$$

$$|\Omega| = 1, \tag{3.3}$$

with $c' = c_2/c_1$ and $\lambda' = \lambda/c_1$. For the remainder of the paper, we will drop the primes for clarity. We refer to appendix A for the computation of c and λ. We only mention that the coefficients satisfy the inequalities (figure 14):

$$0 < c < 1 \quad \text{and} \quad \lambda > 0, \quad \text{for all } d > 0. \tag{3.4}$$

In two dimensions, we can parametrize Ω using polar coordinates: $\Omega = (\cos\theta, \sin\theta)$. In these coordinates, the system (3.1)-(3.3) becomes:

$$\partial_t \rho + \partial_x (\rho \cos\theta) + \partial_y (\rho \sin\theta) = 0, \tag{3.5}$$

$$\partial_t \theta + c\cos\theta \partial_x \theta + c\sin\theta \partial_y \theta + \lambda \left(-\frac{\sin\theta}{\rho}\partial_x \rho + \frac{\cos\theta}{\rho}\partial_y \rho \right) = 0. \tag{3.6}$$

In this section, we suppose that ρ and θ are independent of y, meaning that we are looking at waves which propagate in the x-direction. Under this assumption, the system (3.5),(3.6) reads:

$$\partial_t \begin{pmatrix} \rho \\ \theta \end{pmatrix} + A(\rho, \theta)\, \partial_x \begin{pmatrix} \rho \\ \theta \end{pmatrix} = 0, \tag{3.7}$$

with

$$A(\rho, \theta) = \begin{bmatrix} \cos\theta & -\rho\sin\theta \\ -\frac{\lambda\sin\theta}{\rho} & c\cos\theta \end{bmatrix}. \tag{3.8}$$

The *characteristic velocities* of this system are the eigenvalues of the matrix $A(\rho, \theta)$ explicitly given by

$$\gamma_{1,2} = \frac{1}{2}\left[(c+1)\cos\theta \pm \sqrt{(c-1)^2 \cos^2\theta + 4\lambda\sin^2\theta} \right], \tag{3.9}$$

with $\gamma_1 < \gamma_2$. It is to be noted that the two eigenvalues γ_1 and γ_2 depend only on the angle θ (see figure 1). Since γ_1 and γ_2 are always real and distinct, the system (3.7) is strictly *hyperbolic*. A possible choice of right eigenvectors of $A(\rho, \theta)$ is

$$\vec{r}_1 = \begin{pmatrix} \rho\sin\theta \\ \cos\theta - \gamma_1 \end{pmatrix} \quad \text{and} \quad \vec{r}_2 = \begin{pmatrix} c\cos\theta - \gamma_2 \\ \frac{\lambda\sin\theta}{\rho} \end{pmatrix}. \tag{3.10}$$

The two fields are genuinely nonlinear, i.e. satisfy $\nabla \gamma_p \cdot \vec{r}_p \neq 0$ for $p = 1$ and 2, except at $\theta = 0$, $\theta = \pi$ and at the extrema values of $\gamma_p(\theta)$ which solve:

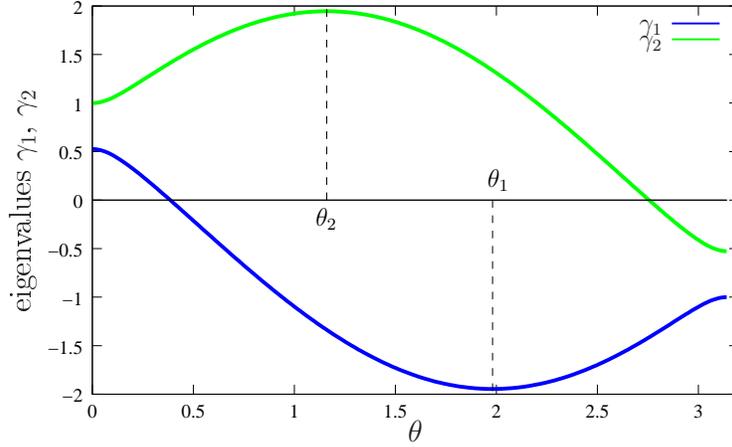$$\tan^2 \theta = \frac{1}{4\lambda} \left[\frac{((c-1)^2 - 4\lambda)^2}{(c+1)^2} - (c-1)^2 \right].$$

Figure 1: The two eigenvalues γ_1 and γ_2 of the matrix $A(\rho, \theta)$ (3.8) depending on θ ($d = 1$ in this graph). For each curve, there exists a unique extremum (θ_1 and θ_2) which corresponds to a linearly degenerate set of the system (e.g. $\nabla \gamma_p \cdot \vec{r}_p = 0$).

We can exhibit the rarefaction waves of the MV model that is a continuous self-similar solution $(\rho(x/t), \theta(x/t))$. With this aim in mind, we first compute the *Riemann invariants* of the system (3.7), which means that we have to find the solutions of the equations:

$$\frac{d\rho}{\rho \sin \theta} = \frac{d\theta}{\cos \theta - \gamma_1} \qquad \text{and} \qquad \frac{d\rho}{c \cos \theta - \gamma_2} = \frac{\rho d\theta}{\lambda \sin \theta}.$$

Integrating these equations, we find the Riemann invariants I_1 and I_2:

$$I_1 = \ln \rho - \int_{\theta_0}^{\theta} \frac{\sin s}{\cos s - \gamma_1(s)} \, ds \quad , \quad I_2 = \ln \rho - \int_{\theta_0}^{\theta} \frac{c \cos s - \gamma_2(s)}{\lambda \sin s} \, ds.$$

From the Riemann invariants I_1 and I_2, we deduce the *integral curves* of the system denoted by $\mathcal{R}_1$ and $\mathcal{R}_2$. These curves are collinear to the vector fields $\vec{r}_1$ and $\vec{r}_2$ respectively and they are constant along the Riemann invariants. We deduce that the integral curves starting from (ρ_ℓ, θ_ℓ) are given by

$$\rho_1(\theta) \;=\; \rho_\ell \exp \left(\int_{\theta_\ell}^{\theta} \frac{\sin s}{\cos s - \gamma_1(s)} \, ds \right), \tag{3.11}$$

$$\rho_2(\theta) \;=\; \rho_\ell \exp \left(\int_{\theta_\ell}^{\theta} \frac{c \cos s - \gamma_2(s)}{\lambda \sin s} \, ds \right). \tag{3.12}$$

From the integral curves $\mathcal{R}_1$ and $\mathcal{R}_2$, we deduce the rarefaction waves of our system (3.7) (see [28, 29, 34]).

3.2   A conservative form of the MV model in one dimension

The MV model is not conservative thus making its analysis both theoretically and numerically difficult. However, in the present case, a conservative formulation of the MV model can be found in one dimension. It is indeed an easy matter to see that the system (3.7) can be rewritten as:

$$|\sin\theta| \left[\partial_t \begin{pmatrix} \rho \\ f_1(\theta) \end{pmatrix} + \partial_x \begin{pmatrix} \rho\cos\theta \\ cf_2(\theta) - \lambda\ln(\rho) \end{pmatrix} \right] = 0, \tag{3.13}$$

with

$$f_1(\theta) = \ln\left|\tan\frac{\theta}{2}\right| = \ln\left|\frac{\sin\theta}{\cos\theta+1}\right|, \tag{3.14}$$

$$f_2(\theta) = \ln|\sin\theta|. \tag{3.15}$$

Thus, in domains where θ satisfies $\sin\theta \neq 0$, the system (3.7) is equivalent to the conservative system:

$$\partial_t \begin{pmatrix} \rho \\ f_1(\theta) \end{pmatrix} + \partial_x \begin{pmatrix} \rho\cos\theta \\ cf_2(\theta) - \lambda\ln(\rho) \end{pmatrix} = 0. \tag{3.16}$$

This formulation will be used in the next section to define a numerical scheme in the "conservative variables" $(\rho, f_1(\theta))$.

Remark.   The conservative formulation of the MV model (3.16) can be also used to define analytically the shock waves of the MV model using the so-called Rankine-Hugoniot conditions. Two states (ρ_ℓ, θ_ℓ) and (ρ_r, θ_r) are connected by a shock wave traveling at a constant speed s if they satisfy:

$$s \begin{pmatrix} \rho_r - \rho_\ell \\ f_1(\theta_r) - f_1(\theta_\ell) \end{pmatrix} = \begin{pmatrix} \rho_r\cos\theta_r - \rho_\ell\cos\theta_\ell \\ cf_2(\theta_r) - cf_2(\theta_\ell) - \lambda\ln\rho_r + \lambda\ln\rho_\ell \end{pmatrix}. \tag{3.17}$$

and usual entropic conditions enables to select the entropic shock waves [28]. However, the conservative formulation (3.16) has been obtained from the MV model (3.5),(3.6) by dividing by $\sin\theta$. This manipulation can change the discontinuous solutions of the system. In other words, the shock waves of the conservative system (3.16) may be not the same as the one of the original non-conservative MV model [29].

3.3   The MV model as the relaxation limit of a conservative system

As discussed in the remark above, the MV model and its conservative formulation may have different solutions. For this reason, it is preferable to develop alternative methods to study the MV model.

In this second approach, we approximate the geometric constraint ($|\Omega| = 1$) by a relaxation term. To be precise, we introduce the relaxation model:

$$\partial_t \rho^\eta + \nabla_x \cdot (\rho^\eta \Omega^\eta) = 0, \tag{3.18}$$

$$\partial_t (\rho^\eta \Omega^\eta) + c \nabla_x \cdot (\rho^\eta \Omega^\eta \otimes \Omega^\eta) + \lambda \nabla_x \rho^\eta = \frac{\rho^\eta}{\eta}(1 - |\Omega^\eta|^2)\Omega^\eta, \tag{3.19}$$

where now Ω^η belongs to $\mathbb{R}^2$. The relaxation operator is the right-hand side of the equation (3.19). This operator forces $|\Omega^\eta|$ to relax to 1. In particular, in the limit η tends to 0, we have formally that $|\Omega^0| = 1$. Yet we have even more thanks to the following proposition.

Proposition 3.1 *The relaxation model (3.18),(3.19) converges to the MV model (3.1)-(3.3) as η goes to zero.*

Proof (formal).   We suppose that ρ^η and Ω^η converge as η goes to zero:

$$\rho^\eta \xrightarrow{\eta \to 0} \rho^0 \quad , \quad \Omega^\eta \xrightarrow{\eta \to 0} \Omega^0.$$

We define $R^\eta = \rho^\eta(1 - |\Omega^\eta|^2)\Omega^\eta$. By assumption, the left-hand side of equation (3.19) is bounded independently of η, therefore multiplying equation (3.19) by η and taking the limit $\eta \to 0$ yields $R^\eta \xrightarrow{\eta \to 0} 0$. This implies that $|\Omega^0|^2 = 1$ (except where $\rho^0 \Omega^0 = 0$ which one assumes to be a negligible set). In particular, we have:

$$\partial_t \Omega^0 \cdot \Omega^0 = 0 \quad , \quad (\Omega^0 \cdot \nabla_x)\Omega^0 \cdot \Omega^0 = 0. \tag{3.20}$$

By definition of R^η, we have $R^\eta \times \Omega^\eta = 0$, thus equation (3.19) leads to:

$$(\partial_t (\rho^\eta \Omega^\eta) + c \nabla_x \cdot (\rho^\eta \Omega^\eta \otimes \Omega^\eta) + \lambda \nabla_x \rho^\eta) \times \Omega^\eta = 0.$$

Consequently, when $\eta \to 0$, we find:

$$\partial_t \left(\rho^0 \Omega^0\right) + c \nabla_x \cdot \left(\rho^0 \Omega^0 \otimes \Omega^0\right) + \lambda \nabla_x \rho^0 = \alpha \Omega^0, \tag{3.21}$$

for a real number α to be determined. Taking the scalar product of (3.21) with Ω^0 and using (3.20) yields:

$$\alpha = \partial_t \rho^0 + c \nabla_x \cdot (\rho^0 \Omega^0) + \lambda \nabla_x \rho^0 \cdot \Omega^0.$$

Using the conservation of mass ($\partial_t \rho^0 = -\nabla_x \cdot (\rho^0 \Omega^0)$), we finally have:

$$\alpha = (c-1)\nabla_x \cdot (\rho^0 \Omega^0) + \lambda \nabla_x \rho^0 \cdot \Omega^0.$$

Therefore, the relaxation term satisfies:

$$\frac{1}{\eta} R^\eta = \left[(c-1)\nabla_x \cdot (\rho^0 \Omega^0) + \lambda \nabla_x \rho^0 \cdot \Omega^0\right]\Omega^0 + O(\eta).$$

Inserting this expression in (3.18),(3.19) yields the MV model (3.1)-(3.3) at the first order in η. $\qquad\square$

The proposition 3.1 shows that the MV model (3.1)-(3.3) can be seen as the relaxation limit of a conservative hyperbolic model with a relaxation term (3.18),(3.19). This link will be used later on to build a numerical scheme. The idea is to solve numerically the system (3.18),(3.19) in the limit $\eta \to 0$.

Remark. As for the MV model, we analyze the hyperbolicity of the relaxation model (3.18),(3.19). The characteristic velocities are given by:

$$\gamma_1 = cu - \sqrt{\Delta} \quad , \quad \gamma_2 = cu \quad , \quad \gamma_3 = cu + \sqrt{\Delta},$$

where u denotes the x-coordinate of Ω^η and $\Delta = \lambda - (c - c^2)u^2$. We deduce that the relaxation model is hyperbolic if and only if

$$|\Omega^\eta| < \sqrt{\frac{\lambda}{c - c^2}}. \tag{3.22}$$

As we can see in figure 2, the quantity $\sqrt{\frac{\lambda}{c-c^2}}$ is greater than 1 for any value of the noise parameter d. Consequently, the relaxation model is hyperbolic for every $|\Omega^\eta| \leq 1$. Since at the limit $\eta \to 0$, $|\Omega^\eta|$ converges to 1, the relaxation model is hyperbolic for any d in this limit.

4 One-dimensional numerical simulations of the MV model

We propose four different numerical schemes to solve the MV model based on the different formulations of the MV model presented in the previous section. Since the system is non-conservative, the schemes are not expected to capture the same discontinuous solutions.
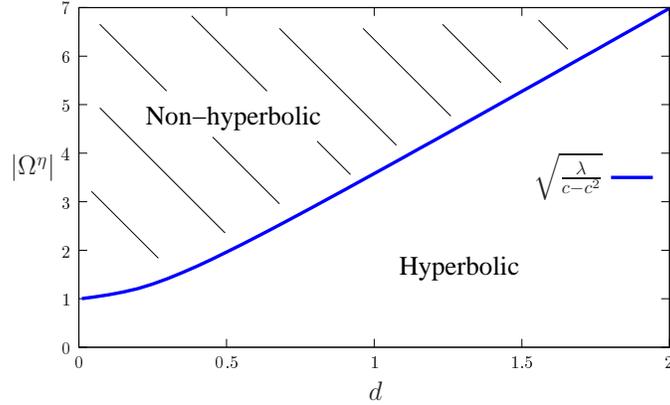
Figure 2: The quantity $\sqrt{\lambda/(c - c^2)}$ depending on d.   The relaxation model (3.18),(3.19) is hyperbolic when the speed $|\Omega^\eta|$ is below this curve.

4.1   Numerical schemes

We use the following notations: we fix a uniform stencil $\{x_i\}_i$ (with $|x_{i+1} - x_i| = \Delta x$) and a time step Δt. For any quantity u, we denote by u_i^n its value at position x_i and time $n\Delta t$.

4.1.1   The splitting method

Our first scheme is based on the relaxation model (3.18),(3.19).   We propose a numerical scheme to solve this system for any η. The idea is to split the relaxation model in two parts. At each time step, we first solve the conservative part:

$$\begin{aligned}
&\partial_t \rho + \nabla_x \cdot (\rho\Omega) = 0, \\
&\partial_t (\rho\Omega) + c\nabla_x \cdot (\rho\Omega \otimes \Omega) + \lambda \nabla_x \rho = 0,
\end{aligned} \tag{4.1}$$

and then the relaxation part:

$$\begin{aligned}
\partial_t \rho &= 0, \\
\partial_t (\rho\Omega) &= \frac{\rho}{\eta}(1 - |\Omega|^2)\Omega.
\end{aligned} \tag{4.2}$$

The conservative part (4.1) is a classical system of conservation laws. We use a Roe method to solve this system with a Roe matrix computed following [29, p. 156].

The relaxation part (4.2) reduces to: $\partial_t \Omega = \frac{1}{\eta}(1 - |\Omega|^2)\Omega$. Since this equation only changes the vector field Ω in norm (i.e. $\partial_t \Omega \cdot \Omega^\perp = 0$), we can once again reduce this equation to:

$$\frac{1}{2}\partial_t |\Omega|^2 = \frac{1}{\eta}(1 - |\Omega|^2)|\Omega|^2. \tag{4.3}$$

Equation (4.3) is solved explicitly: $|\Omega|^2 = (1 + C_0 \, e^{-2/\eta \, t})^{-1}$ with $C_0 = \left(\frac{1}{|\Omega_0|^2} - 1\right)$. Numerically, we just take the limit $\eta \to 0$ of this expression. Therefore, the relaxation part (4.2) yields a mere normalization:

$$\Omega^{n+1} = \frac{\Omega^n}{|\Omega^n|}. \tag{4.4}$$

4.1.2 The conservative scheme

For our second numerical scheme, we use the conservative form of the MV model (3.16):

$$\partial_t V + \partial_x F(V) = 0,$$

with $V = (\rho, f_1(\theta))^T$ and $F(V) = (\rho \cos \theta, \, c f_2(\theta) - \lambda \ln(\rho))^T$. We use a Roe method to discretize this equation:

$$\frac{V_i^{n+1} - V_i^n}{\Delta t} + \frac{\widehat{F}_{i+1/2} - \widehat{F}_{i-1/2}}{\Delta x} = 0, \tag{4.5}$$

where the intermediate flux $\widehat{F}_{i+1/2}$ is given by:

$$\widehat{F}_{i+1/2} = \frac{F(V_i) + F(V_{i+1})}{2} - \left|\mathcal{A}(V_{i+1/2})\right| \frac{V_{i+1} - V_i}{2}. \tag{4.6}$$

Here, $\mathcal{A}$ is the Jacobian of the flux F calculated at the mean value $V_{i+1/2} = \frac{V_i + V_{i+1}}{2}$ and $|\mathcal{A}|$ is the absolute value[1] of the matrix $\mathcal{A}$. Using that $df_1 = (1/\sin \theta) d\theta$ and $df_2 = (\cos \theta / \sin \theta) d\theta$, the Jacobian is explicitly given by:

$$\mathcal{A}(V) = DF(V) = \begin{bmatrix} \cos \theta & -\rho \sin^2 \theta \\ -\frac{\lambda}{\rho} & c \cos \theta \end{bmatrix}.$$

As mentioned earlier, the conservative form is only valid in domains where θ does not cross a singularity $\theta = 0$ or $\theta = \pi$ (i.e. $\sin \theta = 0$). Thus, the conservative form cannot be directly used if $\sin \theta(x)$ changes sign (i.e. there exists x_1 and x_2 such that $\sin \theta(x_1) > 0$ and $\sin \theta(x_2) < 0$). Nevertheless, since the system (3.16) only contains even functions of θ, the conservative formulation (4.5) can be considered as an equation for the absolute value $|\theta|$. To determine the sign of θ, we use an auxiliary scheme such as the upwind scheme defined later on (see section 4.1.3). More precisely, at each time step, $\theta_{\text{cons}}^{n+1}$ and θ_{up}^{n+1} are computed from (ρ^n, θ^n) using respectively the conservative scheme (4.5) and the upwind scheme (4.7) and the new updated value is then given by: $\theta^{n+1} = \text{sign}(\theta_{\text{up}}^{n+1}) |\theta_{\text{cons}}^{n+1}|$.

---

[1]If $\mathcal{A} = R^{-1} D R$ is a diagonalization of $\mathcal{A}$ with $D = \text{diag}(\gamma_1, \gamma_2)$, then $|\mathcal{A}| = R^{-1} |D| R$ with $|D| = \text{diag}(|\gamma_1|, |\gamma_2|)$.

4.1.3 Non-conservative schemes

We present two other numerical schemes based on the non-conservative formulation of the MV model (3.7).

(i) Upwind scheme

The method consists to update the value of $U_i^n = (\rho_i^n, \theta_i^n)$ with the formula:

$$\frac{U_i^{n+1} - U_i^n}{\Delta t} + A^+ \left(\frac{U_i^n - U_{i-1}^n}{\Delta t} \right) + A^- \left(\frac{U_{i+1}^n - U_i^n}{\Delta t} \right) = 0, \tag{4.7}$$

with $A^+ = \frac{A+|A|}{2}$ the positive part of A and $A^- = \frac{A-|A|}{2}$ its negative part.

(ii) Semi-conservative scheme

The upwind scheme has one major problem, it does not conserve the total mass $(\int_x \rho(x)\, dx)$. In order to keep this quantity constant in time, we use the equation of conservation of mass (3.1) in a conservative form:

$$\partial_t \rho + \partial_x H(\rho, \theta) = 0,$$

with $H(\rho, \theta) = \rho \cos \theta$. Therefore, a conservative numerical scheme associated with this equation would be:

$$\frac{\rho_i^{n+1} - \rho_i^n}{\Delta t} + \frac{\widehat{H}_{i+1/2} - \widehat{H}_{i-1/2}}{\Delta x} = 0, \tag{4.8}$$

where $\widehat{H}_{i+1/2}$ is the numerical estimation of the flux H at the interface between x_i and x_{i+1}. To estimate numerically this flux, we use the following formula with $U_i^n = (\rho_i^n, \theta_i^n)$:

$$\widehat{H}_{i+1/2} = H(U_{i+1/2}^n) - |A|_\rho \left(\frac{U_{i+1}^n - U_i^n}{2} \right), \tag{4.9}$$

where the intermediate value is given by $U_{i+1/2} = \frac{U_i + U_{i+1}}{2}$ and $|A|_\rho$ is the first line of the absolute value of A defined above.

For the estimation of the angle θ, we use the upwind scheme. This numerical scheme uses one conservative equation (for the mass ρ) and a non-conservative equation (for the angle θ). It is thus referred to as the *semi-conservative* scheme.

4.2 Numerical simulations

To compare the various numerical schemes, we solve the MV model in 1D (3.7) for various Riemann problems. Thanks to section 3, we can choose a Riemann problem such that the solution consists of a rarefaction wave (figure 3) or a single shock wave (figure 4) using the conservative formulation (3.16). Moreover, we can

compute explicitly the solution of the Riemann problem at any time. Nonetheless, in the case of a shock wave, we have to keep in mind that the theoretical solution has been computed from the conservative formulation (3.16) and *not* from the original MV model (3.7).

We use the following parameters in our simulations: $d = 1$, the computational domain is the interval $[0, 10]$ and the discontinuity for the Riemann problem is at the middle of the domain ($x = 5$). The simulations run for two time units with a time step $\Delta t = 2 \cdot 10^{-2}$ and a space step $\Delta x = 5 \cdot 10^{-2}$. For these values, the Courant number (CFL) is 0.778. We use homogeneous Neumann conditions as boundary conditions.

The first test consists in checking that the numerical schemes coincide on continuous solutions. To obtain a rarefaction wave, we consider the Riemann problem with initial left and right states:

$$(\rho_\ell, \theta_\ell) = (2, 1.7) \quad , \quad (\rho_r, \theta_r) = (1.12, 0.60). \tag{4.10}$$

In figure 3, the numerical solutions of the different schemes are depicted. They all match with each other and agree with the theoretical solution.

The situation is different when we deal with non-smooth solutions such as shock waves, the schemes may provide different solutions. We use as initial condition another Riemann problem:

$$(\rho_\ell, \theta_\ell) = (1, 0.314) \quad , \quad (\rho_r, \theta_r) = (2, 1.54), \tag{4.11}$$

which satisfies the Rankine-Hugoniot condition (3.17). Thus, the theoretical solution, given by the conservative formulation (3.16), is a shock wave connecting the two states. The Rankine-Hugoniot condition (3.17) also gives the theoretical speed of this shock ($s = -.8805$). As we observe in figure 4, the conservative method is in perfect agreement with this theoretical solution, the other schemes give very different solutions. This is not a surprising result since both the theoretical solution and the conservative scheme are based on the same formulation (3.16). Nonetheless, as it has been mentioned before, the theoretical solution of the conservative formulation is not necessarily the correct solutions to the original particle system. In the next section, the particle simulations will show indeed that the right solution for the Riemann problem (4.11) is not given by the conservative method but rather by the splitting method.

5   The microscopic versus macroscopic Vicsek models in 2D

In this section, we would like to validate numerically the MV model by comparing its solutions with the microscopic Vicsek model. First, we make sure that the
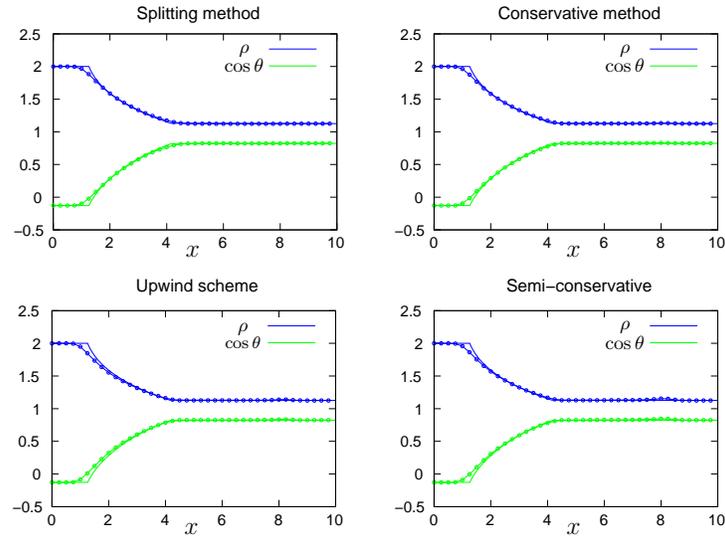
Figure 3: Theoretical solution (solid line) and numerical solutions (points) of the Riemann problem (4.10), ρ (blue) and $\cos\theta$ (green) as functions of space. The simulations run for 2 time units, with a time step $\Delta t = 2 \cdot 10^{-2}$ and a space step $\Delta x = 5 \cdot 10^{-2}$ (CFL=.778).
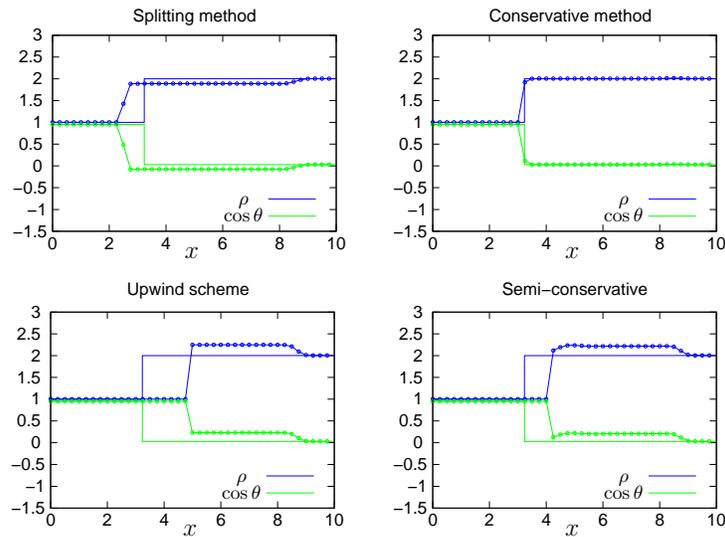

Figure 4: Theoretical solution of the conservative formulation (solid line) and numerical solutions (points) of the Riemann problem (4.11), ρ (blue) and $\cos\theta$ (green) as functions of space. The simulations run for 2 time units, with a time step $\Delta t = 2 \cdot 10^{-2}$ and a space step $\Delta x = 5 \cdot 10^{-2}$ (CFL=.778).

particle's distribution function of the microscopic Vicsek model converges *locally* to an equilibrium as it is predicted by the MV model [16]. Then, we expect that the simulations of the microscopic Vicsek model will be in good agreement with one of the numerical simulations to the MV model. The different numerical schemes of the MV system capture different solutions. However, there is no physical argument that favors one over the others. This section aims at knowing if one of the schemes reproduces the large scale behavior of the particle dynamics. If this is the case, the corresponding scheme will be a way to define the right notion of solution of the MV system.

5.1 Local equilibrium

Like many macroscopic models, the derivation of the MV model is based on the convergence of the particle's distribution function to local equilibrium at large scales in space and time. For the microscopic Vicsek model, these local equilibrium are given by a Von Mises distribution M_Ω [16]:

$$M_\Omega(\omega) = C \exp\left(\frac{\omega \cdot \Omega}{d}\right) \tag{5.1}$$

where C is set by the normalization condition[2]. Here, d is the noise parameter and Ω is the direction of the mean velocity of the particles. The goal of this section is to show numerically that the particle distribution of the microscopic Vicsek model is close in certain regimes to this Von Mises distribution.

With this aim, we have to solve numerically the dynamical system (2.1),(2.2) at large scales in space and time. We introduce the macroscopic variables t' and x' defined as:

$$t' = \varepsilon t \quad, \quad x' = \varepsilon x.$$

Here, ε is the ratio between the microscopic and macroscopic variables. We solve numerically the dynamical system:

$$\frac{dx_k^\varepsilon}{dt} = \omega_k^\varepsilon, \tag{5.2}$$

$$d\omega_k^\varepsilon = \frac{1}{\varepsilon}(\mathrm{Id} - \omega_k^\varepsilon \otimes \omega_k^\varepsilon)(\overline{\omega}_k^\varepsilon \, dt + \sqrt{2d} \, dB_t), \tag{5.3}$$

with $\overline{\omega}_k^\varepsilon$ the average velocity around the particle k,

$$\overline{\omega}_k^\varepsilon = \frac{J_k^\varepsilon}{|J_k^\varepsilon|} \ , \qquad J_k^\varepsilon = \sum_{j, \, |x_j^\varepsilon - x_k^\varepsilon| \le \varepsilon R} \omega_j^\varepsilon. \tag{5.4}$$

---

[2] explicitly given by $C^{-1} = 2\pi \, I_0(d^{-1})$ where I_0 is the modified Bessel function of order 0

Theoretically, the smaller ε is, the closer to the MV model the dynamical system (5.2)-(5.4) would be.

We propose in appendix C a numerical scheme to solve the system (5.2)-(5.4). The scheme is implicit but has the same cost as an explicit scheme. The setting for our particle simulations is as follows: we consider a square box of size L with periodic boundary conditions. As initial condition for the position x_k, we choose a uniform random distribution in space. The velocity ω_k is initially distributed according to a uniform distribution on the unit circle.

We first compare the distribution of the velocity direction θ_k with its theoretical distribution $M_\Omega(\theta)$ given by (5.1). In figure 5, we observe that the two distributions are in good agreement for a certain set of parameters.

To make a systematic comparison between the empirical and theoretical distribution for different parameters, we only consider the mean value of the two distributions in the following. We denote by φ_N the mean velocity of the particles and by φ the mean velocity of the distribution M_Ω:

$$\varphi_N = \frac{1}{N} \left| \sum_{k=1}^{N} \omega_k \right| \quad , \quad \varphi = \left| \int_\omega \omega \, M_\Omega(\omega) \, d\omega \right|. \tag{5.5}$$

We compute the values of φ_N and φ for different values of the noise parameter d. As we can see in figure 6, the two distributions are in close agreement with each other. We also observe a smooth transition from order ($\varphi \approx 1$) to disorder ($\varphi << 1$) as it has been measured in the original Vicsek model [35].

The situation is different when we consider a larger system. The distribution of velocity θ_k may not converge to one *global* equilibrium M_Ω but rather to many *local* equilibrium $M_{\Omega(x)}$. We can no longer ignore the spatial position of the particles x_k. Consequently, the mean velocity of the particles in all the domain φ_N differs from the expected theoretical value φ. We illustrate this phenomena in figure 7: we fix the density of particles and we increase the size of the box. As we observe, the mean velocity φ_N (5.5) has a smaller value when the size of the box L increases. This phenomena has been previously observed in [8]. Now if we reduce ε in the particle simulations, we simulate the dynamical system (2.1)-(2.3) at a larger scale, the size of the box becomes L/ε. Therefore, the agreement between φ_N and φ will surprisingly decrease as ε becomes smaller, although the density of particles is maintained constant.

The mean velocity φ_N also differs from the expected theoretical value φ (5.5) when the density of particles is low. In figure 8, we fix the size of the box ($L = 10$) and we increase the density of particles (the density is given by the number of particles in the circle of interaction). At low density, the mean velocity φ_N is much smaller than the theoretical prediction φ. But as the density of particles increases, the mean velocity φ_N grows and finally converges to φ (see also [35]). For this
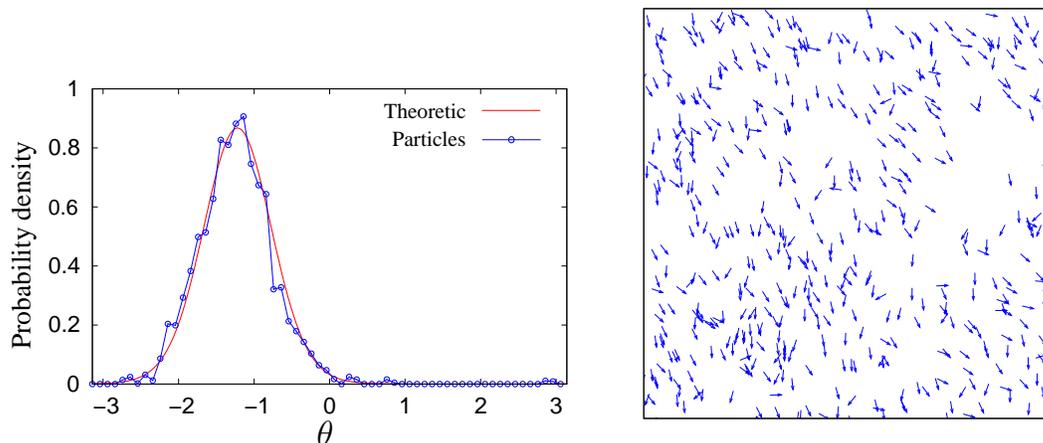
Figure 5: Left figure: the distribution of the velocity direction θ_k (blue), with $\omega_k = (\cos\theta_k, \sin\theta_k)$, compared with the theoretical distribution M_Ω (red) after 6 time units. Right figure: the corresponding particle simulation. Parameters of the simulation: $L = 1$ (box size), number of particles $N = 500$, $\varepsilon = 1/4$, radius of interaction $R = .5$, $d = .2$, $\Delta t = 2 \cdot 10^{-3}$.
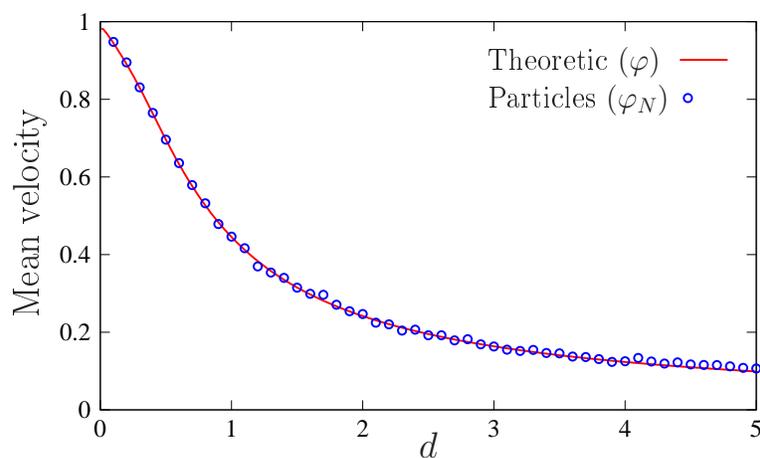

Figure 6: The mean velocity φ_N and φ (5.5) for different values of d. Parameters of the simulation: $L = 1$ (box size), number of particles $N = 200$, $\varepsilon = 1$, $R = .5$, $\Delta t = .02$ time unit, the simulations run for 180 time units.

reason, a dense regime of particles has to be used in the following in order to compare numerically the microscopic model with the MV model.

5.2 Microscopic versus Macroscopic dynamics

We now compare the evolution of the two macroscopic quantities ρ and Ω for the microscopic and macroscopic Vicsek model. We have seen that the different schemes applied to the macroscopic model give different solutions (see figure 4). We expect that the particle simulations will indicate what is the physically relevant solution of the macroscopic model.

We first briefly explain how we proceed to run the particle simulations of a Riemann problem (see also appendix C). We choose a left state (ρ_ℓ, θ_ℓ) and a right state (ρ_r, θ_r), and we distribute a proportion $\frac{\rho_\ell}{\rho_\ell + \rho_r}$ of particles uniformly in the interval $[0, 5]$ and the remaining particles uniformly in the interval $[5, 10]$. Then, we generate the velocities ω_k of the particles according to the distribution M_Ω (5.1) with $\Omega_\ell = (\cos\theta_\ell, \sin\theta_\ell)$ on the left side and $\Omega_r = (\cos\theta_r, \sin\theta_r)$ on the right side. We use the numerical scheme given in appendix C to generate particle trajectories. To make the computation simpler, we choose periodic boundary conditions, thus the number of particles is conserved. As a consequence, there are initially two Riemann problems corresponding to discontinuities at $x = 5$ and at $x = 0$ or 10 (which is the same by periodicity). We use a particle-in-cell method [19, 24] to estimate the two macroscopic quantities: the density ρ and the direction of the flux Ω (which gives θ). In order to reduce the noise due to the finite number of particles, we take a mean over several simulations to estimate the density ρ and θ.

As an illustration, we solve the following Riemann problem:

$$(\rho_\ell, \theta_\ell) = (1, \ 1.5) \quad , \quad (\rho_r, \theta_r) = (2, \ 1.83) \quad , \quad d = 0.2, \tag{5.6}$$

using particle simulations for the microscopic Vicsek model and the splitting method for the MV model. In figure 9, we represent the density ρ for the two solutions in a 2D representation. Since the initial condition is such that the density ρ and the direction θ are independent of the y-direction, we only represent ρ and θ along the x-axis in the following figures. More precisely, for the particle simulations, we take a mean over the y-axis to compute the density distributions, this reduces the noise in the representation. In practice, we simply ignore the y-coordinate of the particles and apply a particle-in-cell method to estimate the density in x. In figure 10, we represent the two solutions (the particle and the macroscopic one) with only a dependence in the x-direction. Three quantities are represented: the density ρ, the flux direction θ and the local temperature T. To estimate $T(x)$, we compute the variance of the velocity distribution around the point x. One can clearly see the propagation of a shock in the middle of the domain and a rarefaction at the
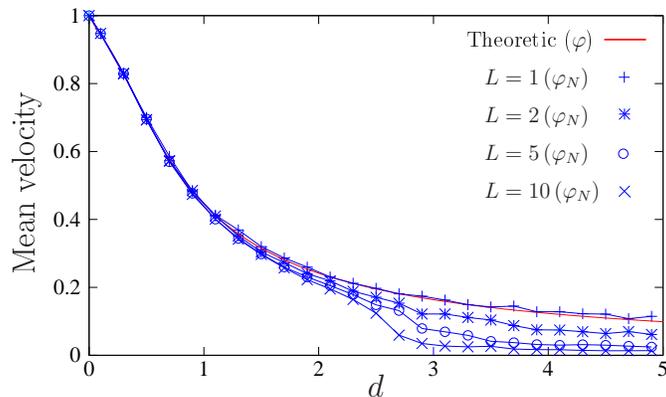
Figure 7: φ_N and φ (5.5) for different values of d and different box sizes L. We keep the same density of particles. As the domain size increases, φ_N decreases which means that particles are less aligned. Parameters of the simulations: $L = 1$, 2, 5, 10 (box size), number of particles $N = 200$, 800, 5000, 20000, $\varepsilon = 1$, $R = .5$, $\Delta t = .02$, the simulations run for 180 time units.
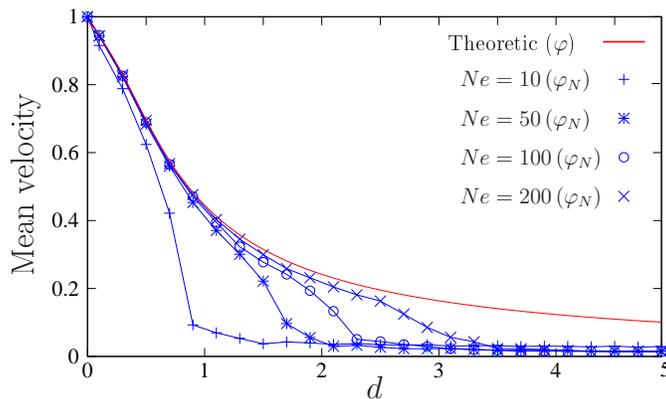

Figure 8: φ_N and φ (5.5) for different values of d and different density of particles. The density is given by the mean number of neighbors Ne of one particle (x_i is a neighbor of x_j if $|x_i - x_j| < R$). As the mean number of neighbors Ne increases, particles are more aligned and φ_N comes closer to φ. Parameters of the simulations: $L = 10$ (box size), number of particles $N = 254$, 1273, 6366, 12732, and 25464, $\varepsilon = 1$, $R = .5$, $\Delta t = .02$, the simulations run for 180 time units.

boundary. The CPU time[3] for one numerical solution at the particle level is about 140 seconds. For the macroscopic model, the CPU time is about 0.1 second which represents a cost reduction of three orders of magnitude. Since we have to take a mean over many particle simulations, the cost reduction is even larger.

Remark.   The macroscopic model supposes that local temperature T is constant everywhere. However, as we can see in figure 10, the temperature (red curve) is larger in regions where the density is lower. A generalization of the MV model has been proposed in [20] to include this effect.

Similarly, we compute the solutions of the Riemann problem (5.6) with the three other numerical schemes and we compare their solution with the particle simulations (figure 11). All the schemes are in good agreement with the microscopic model, we clearly see the propagation of a shock on the left and a rarefaction wave on the right. However, if we look carefully at the shock, we observe that the splitting method is in better agreement with the particle simulations. The propagation of the shock is slightly too slow with the three other schemes.

Now we come back to our previous Riemann problem (4.11) where the four numerical schemes give very different solutions (figure 4). We use a larger domain in x ($L = 20$ space units) in order to avoid the effect of the periodic boundary condition. As we observe in figure 12, the upwind scheme and the semi-conservative method are clearly not in accordance with the particle simulations. Moreover, the splitting method is in better agreement with the particle simulations than the conservative method. The propagation of the discontinuity in the conservative method is too slow compared with the particle simulations.

Our last simulation clearly points out that the splitting method has the best agreement with the particle dynamics. The initial condition consists of a contact discontinuity:

$$(\rho_\ell, \theta_\ell) = (1, 1) \quad , \quad (\rho_r, \theta_r) = (1, -1) \quad , \quad d = 0.2, \tag{5.7}$$

i.e. we reflect the angle with respect to the x-axis across the middle point $x = 5$. A natural (weak) solution for this problem is the contact discontinuity propagating at the speed $c \cos(1)$:

$$\rho(t, x) = 1 \quad , \quad \theta(t, x) = \theta_0(x - c\cos(1)t), \tag{5.8}$$

with $\theta_0(x) = -1$ when $x < 5$ and $\theta_0(x) = 1$ when $x > 5$. This is the solution provided by the conservative scheme (figure 13). But surprisingly, the splitting method and the particle simulations agree on a different solution. Indeed, the solutions given by the particles and the splitting method are in fairly good agreement

---

[3]The computations have been made with an Intel Core Duo T2300 with 1GB of RAM

with each other. This seems to indicate that the "physical solution" to the contact problem (5.7) is not given by the conservative formulation (5.8) but by a much more complex profile. The constraint of unit speed drastically changes the profile of the solution compared with what would be found for a standard system of conservative laws.
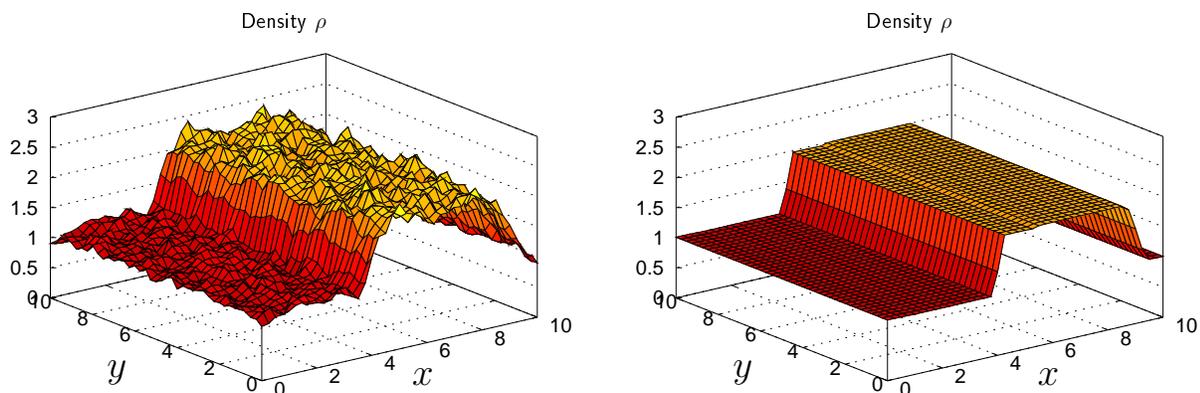
Figure 9: The particle density in space ρ computed with particle simulations (left) and the MV model (right). We initialize with the Riemann problem (5.6). Numerical parameters for the particle simulations: $N = 2 \cdot 10^6$ particles, $\Delta t = .01$, $\varepsilon = 1/10$, $R = .5$, $L = 10$, we take a mean over 10 computations. Numerical parameters for the macroscopic model: $\Delta t = .01$, $\Delta x = .025$ (CFL=0.416), we use the splitting method. The simulations run for 2 time units.
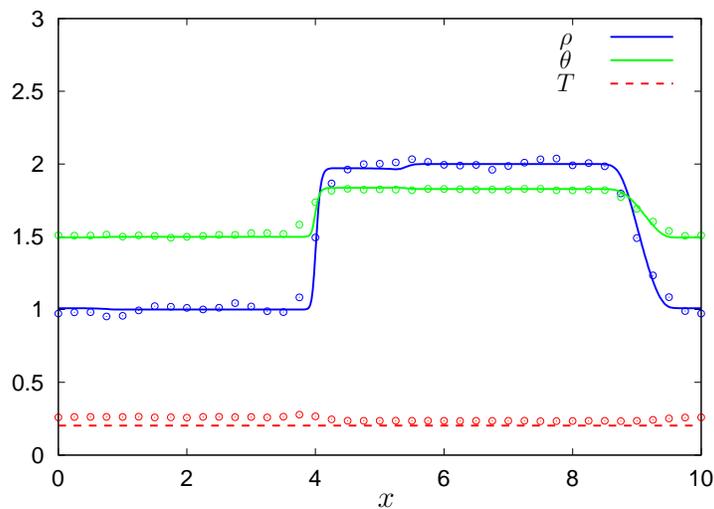

Figure 10: The solution of the Riemann problem (5.6) computed with the splitting method (solid line) and with particle simulations (dots). We represent the density ρ (blue), the flux direction θ (green) and the local temperature T (red). The parameters are the same as in figure 9, we only change the representation of the solution (1D-representation).
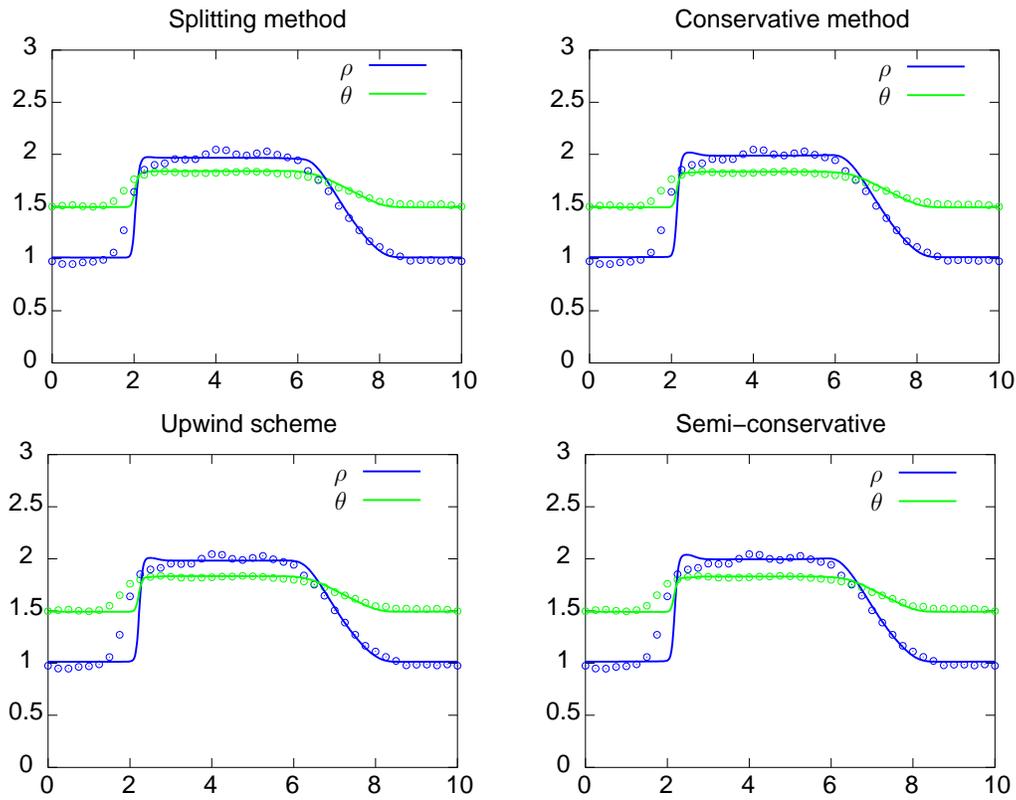
Figure 11: The solutions of the Riemann problem (5.6) computed using the four numerical schemes for the MV model (solid line) and the microscopic model (dots). The parameters are the same as in figure 9. The simulations run for 6 time units.
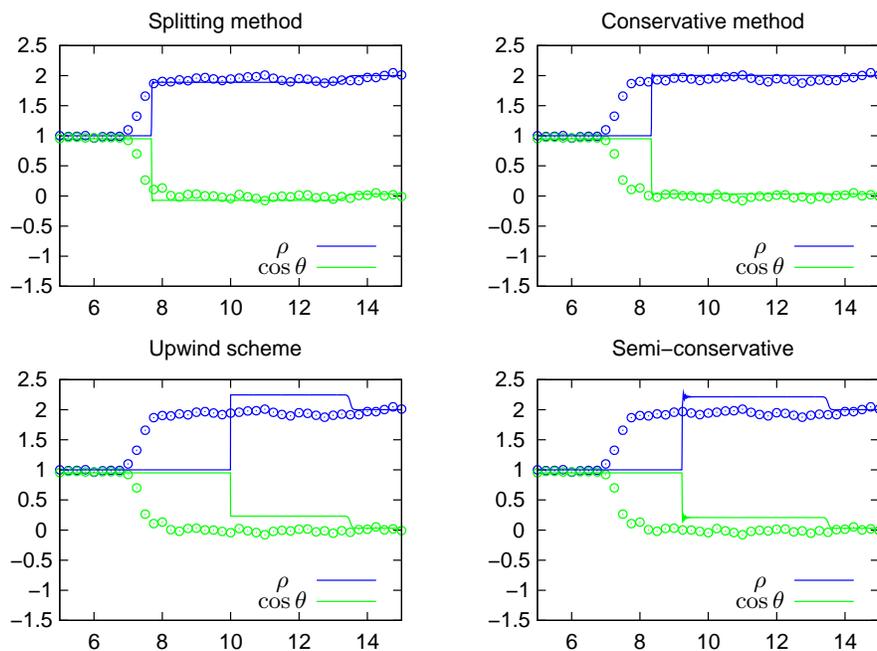
Figure 12: The solutions of the Riemann problem (4.11) computed using the four numerical schemes for the MV model (solid line) and the microscopic model (dots). Numerical parameters for the MV model: $\Delta t = .01$, $\Delta x = .025$ (CFL=0.778). Numerical parameters for the microscopic model: $N = 2 \cdot 10^6$ particles, $\Delta t = .02$, $\varepsilon = 1/10$, $R = .5$, $Lx = 20$ and $Ly = 1$. We take a mean over 50 simulations. The simulations run for 6 time units. Since $d = 1$, fluctuations are higher (see figure 8), we have to increase the density of particles to reduce this effect.
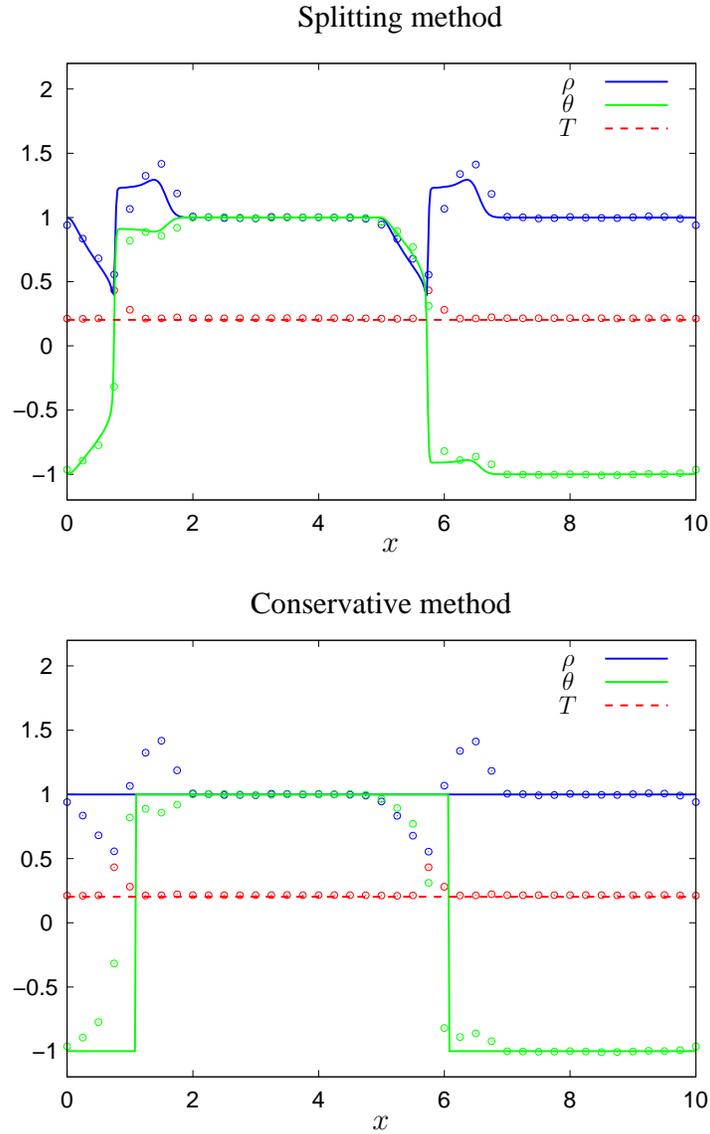
Figure 13: The solution of the Riemann problem (5.7) computed with the splitting method (top), the conservative method (down) and particle simulations (dots). Numerical parameters for the MV model: $\Delta t = .01$, $\Delta x = .025$ (CFL=0.416). Numerical parameters for the microscopic model: $N = 10^6$ particles, $\Delta t = .01$, $\varepsilon = 1/10$, $R = .5$, $Lx = 10$, $Ly = 1$. We take a mean over 100 simulations. The simulations run for 2 time units.

6   Conclusion

In this work, we have studied numerically both the microscopic Vicsek model and its macroscopic version [16]. Due to the geometric constraint on the velocity, the standard theory of hyperbolic systems is not applicable for the macroscopic model. Therefore, we have proposed several numerical schemes to solve this system. By comparing the simulations of the microscopic and macroscopic model, it appears that the scheme based on a relaxation formulation of the macroscopic model, used in conjunction with a splitting method, is in good agreement with particle simulations. The other schemes do not show a similarly good agreement. In particular, with an initial condition given by a contact discontinuity, the microscopic model and the *splitting method* provide a similar solution which turns out to be much more complex than what could be expected.

These results confirm the relevance of the macroscopic Vicsek model. Since the macroscopic model costs much less CPU time, it is an effective tool to simulate the Vicsek dynamics in a dense regime of particles.

Many questions are still open concerning the macroscopic Vicsek model. We have seen that the splitting method gives results which are in accordance with particle simulations. But it remains to be understood why this particular scheme captures the particle dynamics better than the other schemes. Since the macroscopic model has original characteristics, this question is challenging. Another point concerns the particle simulations. We have seen that the density of particles has a strong effect on the "local temperature" (i.e. the variance of the velocity distribution). When the density is low, the temperature is larger. The macroscopic model does not capture this effect, the variance of the velocity distribution is always the same. Works are in progress to understand this effect of the density.

A   The coefficients c_1, c_2 and λ

The macroscopic coefficients of the MV model c_1, c_2 and λ involve two functions: the Von Mises distribution M_Ω (5.1) and the generalized collisional invariant ψ [16]. In two dimensions, $\psi(\theta)$ is a periodic function which satisfies the elliptic equation:

$$\partial_\theta \left(e^{\frac{\cos \theta}{d}} \partial_\theta \psi \right) = \sin \theta e^{\frac{\cos \theta}{d}}. \tag{A.1}$$

Using the notation $M(\theta) = Ce^{\frac{\cos \theta}{d}}$, the coefficients c_1, c_2 and λ are given by:

$$c_1 = \langle \cos \theta \rangle |_M = \int_{-\pi}^{\pi} \cos \theta \, M(\theta) \, d\theta \tag{A.2}$$

$$c_2 = \frac{\langle \cos \theta \, \sin \theta \, \psi \rangle_M}{\langle \sin \theta \, \psi \rangle_M} = \frac{\int_{-\pi}^{\pi} \cos \theta \sin \theta \psi(\theta) M(\theta) \, d\theta}{\int_{-\pi}^{\pi} \sin \theta \psi(\theta) M(\theta) \, d\theta} \tag{A.3}$$

$$\lambda = d, \tag{A.4}$$

where d is the noise parameter. Thus, only c_1 and λ are defined explicitly. For c_2, we need first to solve the equation (A.1) to obtain ψ. Equation (A.1) can be explicitly integrated using that ψ is a periodic function.

Lemma A.1 *The periodic solution ψ of Eq. (A.1) is given by:*

$$\psi(\theta) = d\,\theta - \frac{\int_0^\theta e^{-\frac{\cos s}{d}} \, ds}{\int_0^\pi e^{-\frac{\cos s}{d}} \, ds} + C, \tag{A.5}$$

where C is a constant.

The proof of this lemma is straightforward and omitted. Since we have an explicit expression for both M and ψ, we only have to make a numerical integration to estimate c_1 and c_2. We can also deduce the asymptotic of the coefficients c_1 and c_2 as the parameter d becomes large:

Lemma A.2 *The coefficients c_1 and c_2 defined respectively by the equations (A.2) and (A.3) satisfy the following asymptotic:*

$$c_1 \overset{d \to \infty}{\sim} \frac{1}{2d} + O\left(d^{-2}\right), \qquad c_2 \overset{d \to \infty}{\sim} \frac{3}{16d} + O\left(d^{-2}\right). \tag{A.6}$$

In particular, we have:

$$\frac{c_2}{c_1} \overset{d \to \infty}{\sim} \frac{3}{8} + O(d^{-2}), \qquad \frac{\lambda}{c_1} \overset{d \to \infty}{\sim} 2d^2 + O\left(1\right). \tag{A.7}$$

We omit the proof of this lemma since it only requires to compute the Taylor expansion of the exponential several times. In figure 14, we plot the ratio $c' = c_2/c_1$ and $\lambda' = \lambda/c_2$ for different values of d along with their asymptotic (A.7).
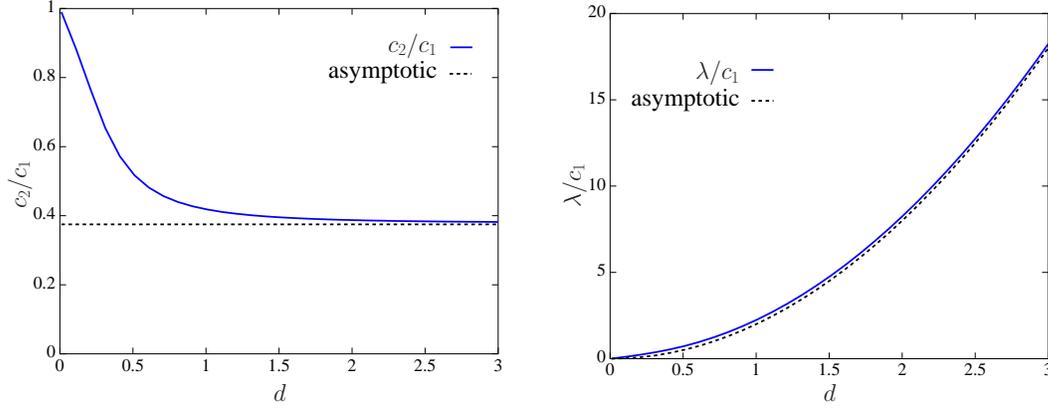
Figure 14: The ratio c_2/c_1 and λ/c_1 (solid lines) for different values of the noise parameter d and their asymptotic (dashed line) as d becomes large (A.7).

B   Special solution of the MV model

In this appendix, a vortex configuration is exhibited as a stationary solution of the MV model (2.4)-(2.6) in two dimensions. A stationary solution of the MV model satisfies:

$$\nabla_x \cdot (\rho\Omega) = 0,$$
$$c(\Omega \cdot \nabla_x)\Omega + \lambda\left(\text{Id} - \Omega \otimes \Omega\right)\frac{\nabla_x\rho}{\rho} = 0. \tag{B.1}$$

To formulate the vortex configuration, we introduce polar coordinates, $\rho(r,\theta)$, $\Omega(r,\theta) = f_r(r,\theta)\vec{e}_r + f_\theta(r,\theta)\vec{e}_\theta$, where $\vec{e}_r = (\cos\theta, \sin\theta)^T$ and $\vec{e}_\theta = (-\sin\theta, \cos\theta)^T$.

Proposition B.1 *The following initial condition is a stationary state of the MV model (B.1):*

$$\rho(r) = C\,r^{c/\lambda} \qquad , \qquad \Omega = \vec{e}_\theta, \tag{B.2}$$

where C is a constant.

Proof. With the expression of ρ and Ω given by (B.2), the divergence of the mass is zero and the gradient of ρ is orthogonal to Ω. Therefore the system (B.1) reduces to:

$$c(\Omega \cdot \nabla_x)\Omega + \lambda\frac{\nabla_x\rho}{\rho} = 0,$$

or in polar coordinates:

$$c\frac{1}{r}\partial_\theta\,\vec{e}_\theta \ + \ \lambda\frac{\rho'(r)}{\rho(r)}\vec{e}_r = 0.$$

Since $\partial_\theta\vec{e}_\theta = -\vec{e}_r$, we can easily check that the solution of this equation is given by $\rho(r) = C\,r^{c/\lambda}$. $\qquad\qquad\square$

C Numerical schemes for particle simulations

An explicit Euler method for the differential system (5.2)-(5.4) would impose a CFL condition $\frac{1}{\varepsilon}\Delta t < 1$. Hence, we would like to find an implicit scheme to solve the system (2.1)-(2.3). With this aim, we use the following discretized formulation of the microscopic Vicsek model (see [16]):

$$\frac{\omega^{n+1} - \omega^n}{\Delta t} = (\mathrm{Id} - \omega^{n+1/2} \otimes \omega^{n+1/2})(\overline{\omega}^n - \omega^n) \qquad (\mathrm{C}.1)$$

where $\omega^{n+1/2} = \frac{\omega^n + \omega^{n+1}}{|\omega^n + \omega^{n+1}|}$ and $\overline{\omega}^n$ is the average velocity (2.3). When $\Delta t = 1$, we recover exactly the original Vicsek model [35]. Equation (C.1) can be solved explicitly. Indeed, since $\omega^{n+1} - \omega^n$ is the orthogonal projection of $(\overline{\omega}^n - \omega^n)\Delta t$ on the orthogonal plane of $\omega^{n+1/2}$, the vectors ω^{n+1} and ω^n belong to the circle $\mathcal{C}$ centered at $B = \omega_n + \frac{(\overline{\omega}^n - \omega^n)\Delta t}{2}$ with radius $\left|\frac{(\overline{\omega}^n - \omega^n)\Delta t}{2}\right|$ (see figure 15). But ω^{n+1} and ω^n also belong to the unit circle ($|\omega^{n+1}| = |\omega^n| = 1$), therefore ω^n and ω^{n+1} are the two intersections of $\mathcal{C}$ with the unit circle. Denoting by θ the angle of the vector ω, this implies:

$$\theta^{n+1} = \theta^n + 2\widehat{(\omega^n, B)}.$$

To take into account the effect of the noise, we simply add a random variable:

$$\theta^{n+1} = \theta^n + 2\widehat{(\omega^n, B)} + \sqrt{2d\,\Delta t}\,\epsilon_n \qquad (\mathrm{C}.2)$$

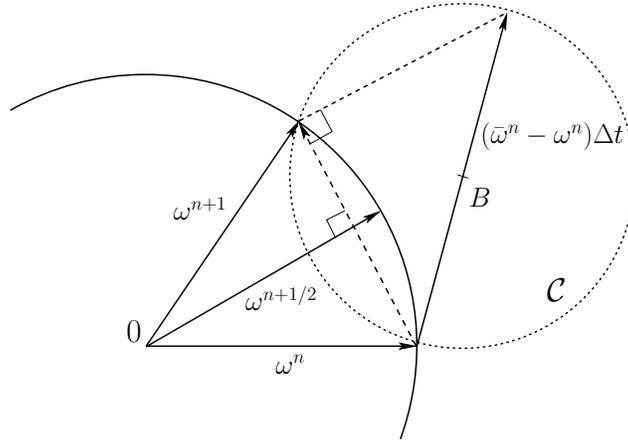where ϵ_n is a random variable independent of θ^n with standard normal distribution.

Figure 15: Illustration of the geometric method to solve explicitly equation (C.1).

References

[1] M. Aldana and C. Huepe. Phase transitions in Self-Driven Many-Particle systems and related Non-Equilibrium models: A network approach. *Journal of Statistical Physics*, 112(1):135–153, 2003.

[2] I. Aoki. A simulation study on the schooling mechanism in fish. *Bulletin of the Japanese Society of Scientific Fisheries (Japan)*, 1982.

[3] M. Ballerini, N. Cabibbo, R. Candelier, A. Cavagna, E. Cisbani, I. Giardina, V. Lecomte, A. Orlandi, G. Parisi, A. Procaccini, et al. Interaction ruling animal collective behavior depends on topological rather than metric distance: Evidence from a field study. *Proceedings of the National Academy of Sciences*, 105(4):1232, 2008.

[4] E. Bertin, M. Droz, and G. Grégoire. Boltzmann and hydrodynamic description for self-propelled particles. *Physical Review E*, 74(2):22101, 2006.

[5] F. Bouchut. *Nonlinear stability of finite volume methods for hyperbolic conservation laws and well-balanced schemes for sources.* Birkhauser, 2004.

[6] J. Buhl, D. J. T. Sumpter, I. D. Couzin, J. J. Hale, E. Despland, E. R. Miller, and S. J. Simpson. *From Disorder to Order in Marching Locusts*, volume 312. American Association for the Advancement of Science, 2006.

[7] M. J Castro, P. G LeFloch, M. L Muñoz-Ruiz, and C. Parés. Why many theories of shock waves are necessary: Convergence error in formally path-consistent schemes. *Journal of Computational Physics*, 227(17):8107âĂŞ8129, 2008.

[8] H. Chaté, F. Ginelli, G. Grégoire, and F. Raynaud. Collective motion of self-propelled particles interacting without cohesion. *Physical Review E*, 77(4):46113, 2008.

[9] G. Q. Chen, C. D. Levermore, and T. P. Liu. Hyperbolic conservation laws with sti relaxation and entropy. *Comm. Pure Appl. Math*, 47:787, 1994.

[10] Y. Chuang, M. R D'Orsogna, D. Marthaler, A. L Bertozzi, and L. S Chayes. State transitions and the continuum limit for a 2D interacting, self-propelled particle system. *Physica D: Nonlinear Phenomena*, 232(1):33–47, 2007.

[11] I. D Couzin, J. Krause, R. James, G. D Ruxton, and N. R Franks. Collective memory and spatial sorting in animal groups. *Journal of Theoretical Biology*, 218(1):1–11, 2002.

[12] F. Cucker and E. Mordecki. Flocking in noisy environments. *Journal de math-ématiques pures et appliquées*, 2007.

[13] F. Cucker and S. Smale. Emergent behavior in flocks. *IEEE Transactions on automatic control*, 52(5):852, 2007.

[14] A. Czirók, A. L Barabási, and T. Vicsek. Collective motion of self-propelled particles: Kinetic phase transition in one dimension. *Physical Review Letters*, 82(1):209–212, 1999.

[15] A. Czirók, H. E Stanley, and T. Vicsek. Spontaneously ordered motion of self-propelled particles. *Journal of Physics A: Mathematical and General*, 30:1375, 1997.

[16] P. Degond and S. Motsch. Continuum limit of self-driven particles with orientation interaction. *Mathematical Models and Methods in Applied Sciences*, 18(1):1193–1215, 2008.

[17] P. Degond and S. Motsch. Large scale dynamics of the persistent turning walker model of fish behavior. *Journal of Statistical Physics*, 131(6):989–1021, 2008.

[18] P. Degond, L. Navoret, R. Bon, and D. Sanchez. Congestion in a macroscopic model of self-driven particles modeling gregariousness. *Journal of Statistical Physics*, pages 1–41, 2009.

[19] H. Fehske, R. Schneider, and A. Weisse. *Computational Many-Particle Physics*. Springer Verlag, 2007.

[20] A. Frouvelle. A continuous model for alignment of self-propelled particles with anisotropy and density-dependent parameters. *Arxiv preprint arXiv:0912.0594*, 2009.

[21] J. Gautrais, C. Jost, M. Soria, A. Campo, S. Motsch, R. Fournier, S. Blanco, and G. Theraulaz. Analyzing fish movement as a persistent turning walker. *Journal of Mathematical Biology*, 58(3):429–445, 2009.

[22] G. Grégoire and H. Chaté. Onset of collective and cohesive motion. *Physical Review Letters*, 92(2):25702, 2004.

[23] S. Y Ha and E. Tadmor. From particle to kinetic and hydrodynamic descriptions of flocking. *Kinetic and Related Models*, 1(3):415–435, 2008.

[24] R. W Hockney and J. W Eastwood. *Computer Simulation Using Particles*. Institute of Physics Publishing, 1988.

[25] T. Y Hou and P. G Le Floch. Why nonconservative schemes converge to wrong solutions: error analysis. *Mathematics of Computation*, 62(206):497–530, 1994.

[26] A. Huth and C. Wissel. The simulation of the movement of fish schools. *Journal of theoretical biology*, 156(3):365–385, 1992.

[27] P. L LeFloch. Entropy weak solutions to nonlinear hyperbolic systems under nonconservative form. *Communications in Partial Differential Equations*, 13(6):669–727, 1988.

[28] R. J LeVeque. *Numerical Methods for Conservation Laws*. Birkhäuser, 1992.

[29] R. J LeVeque and MyiLibrary. *Finite volume methods for hyperbolic problems*. Cambridge University Press, 2002.

[30] A. Mogilner and L. Edelstein-Keshet. A non-local model for a swarm. *Journal of Mathematical Biology*, 38(6):534–570, 1999.

[31] M. Nagy, I. Daruka, and T. Vicsek. New aspects of the continuous phase transition in the scalar noise model (SNM) of collective motion. *Physica A: Statistical Mechanics and its Applications*, 373:445–454, 2007.

[32] C. W Reynolds. Flocks, herds and schools: A distributed behavioral model. In *ACM SIGGRAPH Computer Graphics*, volume 21, pages 25–34, 1987.

[33] C. M Topaz, A. L Bertozzi, and M. A Lewis. A nonlocal continuum model for biological aggregation. *Bulletin of Mathematical Biology*, 68(7):1601–1623, 2006.

[34] E. F Toro. *Riemann solvers and numerical methods for fluid dynamics*. Springer New York, 1997.

[35] T. Vicsek, A. Czirók, E. Ben-Jacob, I. Cohen, and O. Shochet. Novel type of phase transition in a system of self-driven particles. *Physical Review Letters*, 75(6):1226–1229, 1995.